AAEC/E420

AAEC/E420

AUSTRALIAN ATOMIC ENERGY COMMISSION

RESEARCH ESTABLISHMENT

LUCAS HEIGHTS

A TIME-OF-FLIGHT MEASUREMENT SYSTEM USING THE ELEVATED TARGET FACILITY FOR THE AAEC 3 MV VAN DE GRAAFF ACCELERATOR

by

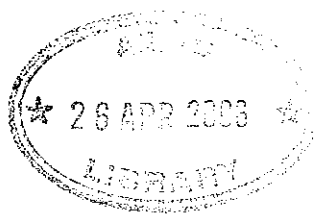

S. WHITTLESTONE

September 1977

ISBN 0 642 59621 2

AAEC-E-420

AUSTRALIAN ATOMIC ENERGY COMMISSION
RESEARCH ESTABLISHMENT
LUCAS HEIGHTS

A TIME-OF-FLIGHT MEASUREMENT SYSTEM USING THE ELEVATED TARGET FACILITY FOR THE AAEC 3 MV VAN DE GRAAFF ACCELERATOR

by

S. WHITTLESTONE

ABSTRACT

A neutron time-of-flight measuring system is described. A 3 MV Van de Graaff accelerator is equipped with a beam pulsing system which can produce pulses as narrow as 3 ns FWHM with residual beam less than 10^{-4} times the peak current. An elevated target station reduces scattered neutron and gamma-ray background by more than a factor of four compared with a conventional near-ground location.

Neutrons are detected by an NE213 scintillator, for which construction and calibration details are given. A computer-based control and data acquisition system allows automatic measurements of angular distributions.

National Library of Australia card number and ISBN 0 642 59621 2

The following descriptors have been selected from the INIS Thesaurus to describe the subject content of this report for information retrieval purposes. For further details please refer to IAEA-INIS-12 (INIS: Manual for Indexing) and IAEA-INIS-13 (INIS: Thesaurus) published in Vienna by the International Atomic Energy Agency.

TIME-OF-FLIGHT METHOD; TIME-OF-FLIGHT SPECTROMETERS; NEUTRON SCINTILLATION DETECTORS; VAN DE GRAAFF ACCELERATORS; BERYLLIUM 9 TARGET; BEAM TRANSPORT

CONTENTS

1. INTRODUCTION

Time-of-flight measurement is a well established technique, either for measuring the energy spectrum of a neutron source or for selecting from a neutron source neutrons of a particular energy. This report describes a time-of-flight system which has been used both to measure the energy spectrum of the thick target ^{9}Be(d,n) source [Whittlestone 1976, 1977] and to select neutrons of well-defined energies from this source, in order to measure pulse height profiles of organic scintillator neutron detectors.

The basis of this system is the 3 MV Van de Graaff accelerator at the AAEC Research Establishment, Lucas Heights; the accelerator can produce beam pulses 3 ns wide FWHM and 1 mA peak current. The charged particle beam can be transported to an elevated target station where background due to neutron scattering from the floor is virtually eliminated. Background from residual beam, which is present in the nominally 'off' state of the pulsing system, is reduced to a very small level by a post acceleration deflection (PAD) system installed close to the base of the accelerator pressure tank.

Details are given of the performance of the pulsing system and reduction in neutron and gamma background achieved using the elevated target facility. The technique for determining the energy dependent efficiency of the NE213 liquid scintillator detector (manufactured by Nuclear Enterprises Limited, Edinburgh, Scotland) used to measure the Be(d,n) source spectra is described together with details of detector chamber design and filling methods. Some special features, such as computer control of the time-of-flight experiment, are also described.

2. THE BEAM PULSING SYSTEM

2.1 High Voltage Terminal Pulser

The beam pulser, located in the high voltage terminal of the accelerator, consists of a standard deflection chamber (High Voltage Engineering Corporation, Part No. D-KTU-35) with two orthogonal sets of deflection plates which can deflect the beam away from a 2.4 mm chopping aperture. A 1 MHz 3.5 kV peak-to-peak (p-p) signal supplied to the first set of plates produces pulses of about 12-15 ns FWHM once every 500 ns. The ratio of peak current to steady background current is about 100:1. For most experiments, a larger interval between pulses is required, so a voltage is applied between a second set of deflection plates to eliminate unwanted pulses. There are two systems available for this.

One uses a 900 V p-p, 1 MHz signal to produce a beam pulse every microsecond; the other uses a 1 kV bistable multivibrator, switched externally, to provide pulses separated by an interval which can be any multiple of 0.5 μs greater than 1.5 μs.

After emerging from the deflection chamber, the beam passes through a klystron buncher which, under favourable conditions, can reduce the beam pulse width to less than 3 ns [Moak *et al.* 1967]. The pulsing system has been described by Ritchie & Fraser [1973].

2.2 Post Acceleration Deflection System

For many experiments, the relatively high, slowly varying background current (up to 2 per cent of the peak current) from the high voltage terminal pulser is undesirable. It creates a need for complex background subtraction procedures in time-of-flight measurements [Whittlestone 1976]. This background has been reduced by use of a PAD system. The deflection plates have been installed to deflect the beam at right angles to the analysing magnet deflection plane to avoid interaction with the beam energy stabilising system.

The present PAD is an improved version of one described by Fraser *et al.* [1968]. Fast rise times (150 ns, 10 to 90 per cent) have been achieved by the circuit shown schematically in Figure 1. In its quiescent *BEAM OFF* state, both valves, V1 and V2, are biased off and 5 kV is maintained at the output by the screen supply circuit of V1. To achieve transition to the *BEAM ON* state, a start pulse activates a drive unit which provides a stepped pulse (Figure 1), driving V2 to draw up to 5 A for 150 ns, and thereafter maintaining the valve in a conducting state with considerably lower power dissipation. This effectively discharges the capacitance of the deflection plates (~ 100 pF) in 150 ns and keeps the anode voltage slightly above the screen voltage. When a stop pulse is provided, V2 is biased off and, after a delay of about 100 ns, V1 is turned on for 150 ns, thus recharging the deflection plate capacitance and returning the system to its quiescent *BEAM OFF* state.

Two modes of operation are possible with this system. When beam pulses wider than about 1 μs are required, square pulses are produced at one deflection plate and the bias plate voltage is adjusted so that the beam can pass through to the target for the duration of the pulse. This mode is unsuitable for residual beam suppression in time-of-flight experiments, because the narrowest pulse width from the PAD is a few hundred nanoseconds. In the second mode of operation, therefore, the

bias plate is set to 3 kV and the start pulse timed to let the pulse from the accelerator pass through when the deflection plate reaches 3 kV, during its sweep from 6 to 0.8 kV. Similarly, the stop pulse is timed to let a beam pulse through during the return sweep from 0.8 to 6 kV.

The latter mode of operation has successfully suppressed background from residual beam when the accelerator pulsing system is operated in the bunched mode. Figure 2(a) shows the beam pulse profile produced from measurements, by a plastic scintillation detector, of γ-rays emitted when the beam pulse hits the target. The background level, 30 ns after the peak, was less than 10^{-4} of the peak. A more direct measurement of the time window, during which the PAD permitted beam to reach the target, was made by using a steady beam from the accelerator and operating the PAD. The pulse width was 24 ns FWHM and the residual beam level was less than 10^{-3} at 40 ns (Figure 2(b)).

An unfortunate characteristic of this type of device is the production of a large quantity of radio-frequency radiation that can be picked up by sensitive detectors. In spite of extensive use of insulated joints and earth straps, the beam line in which the deflection chamber was installed remained a source of interference. This problem has since been largely eliminated by installing a 30 cm section of Pyrex tube in the beam line immediately after the post-acceleration deflection chamber.

3. ELEVATED TARGET FACILITY

3.1 Beam Transport and Energy Stabilisation

A photograph of the elevated target facility is shown in Figure 3. The beam from the accelerator is conducted through two 45° bending magnets (M_1 and M_2) and the quadrupole focusing magnet (Q) to the target station, which is 5 m above the floor. To avoid problems of beam alignment with different loadings, the support towers are designed to deflect by less than 0.1 mm under a vertical load of 1000 kg.

Energy stabilisation of the accelerator beam can be achieved by using as input to the corona stabiliser the difference signal from the slit system at S1, which is on a short section of flight tube set at 32.5° to the undeflected beam axis, thereby using the double mass components (H_2^+ or D_2^+) from the ion source. This avoids loss of beam which would be incurred by insertion of a slit system in the main beam line. When the PAD system is used (Section 2), however, the mass 2 component, being slower, is eliminated and the beam energy is stabilised using a

second set of slits (S2). This has the disadvantage that the magnet flux cannot be used as an accurate indication of beam energy because there is a range of flux settings for the two magnets which permits a beam of a particular energy through to the target. Under these circumstances, the beam energy is read with an accuracy of about ± 5 keV from a generating voltmeter monitoring the potential of the high voltage terminal. If better accuracy were required, a third slit system could be installed just before the quadrupole focusing magnet.

3.2 Reduction of Neutron and Gamma-ray Background when using the Elevated Target Facility

Experiments using the elevated target facility (ELF) avoid the analytical difficulties and uncertainties associated with neutron and gamma-ray scattering within a few metres of the target. The advantages of using the ELF, rather than a standard target station which is typically about 1 m above the floor (the 'floor' target) were studied in an experiment in which scattered neutrons and gamma rays were clearly distinguishable from those arriving directly from the target.

Thin ($\lesssim$ 10 keV) lithium metal targets were mounted at each of the target stations, and a 36 m x 50 m diameter NE213 scintillator detector was set up at 0° to the beam direction and 1.033 m from each target in turn. With an incident proton energy of 2.3 MeV in both cases, the energy of neutrons travelling directly from the target to the detector was in the range 560 to 570 keV. At each target station, a dual parameter experiment was carried out in which pulse height spectra as a function of time were measured, as well as the time spectra of events occurring in the detector. The time spectra measured at the ELF and floor stations are shown in Figure 4; the heavy lines indicate the time windows in which pulse height spectra were also measured.

The apparent inconsistency of the leading and trailing edges of the gamma flash with the sharp rise and fall times of the neutron peak arose, in each case, from gamma rays generated as the PAD system swept the beam across the aperture nearest to the target. Since no neutrons are generated by protons hitting the aperture edges, these wings on the gamma flash profiles have no bearing on the analysis of the time spectra at later times.

Those features of Figure 4 relevant to the discussion of the advantages of the ELF over the floor target appear at times later than the point marked (a). This point corresponds to the earliest time at

which neutrons produced in the beam pulse reach the detector after scattering from the floor in the vicinity of each target. The time can easily be estimated from a knowledge of the total path length and the neutron energy, which depends on the angle of emission from the target. No correction was made for the relatively small amount of energy lost by neutrons scattered by the concrete of the floor and by the iron tower supporting the ELF target.

It can be seen from Figure 4 that at point (a) there is a marked change of slope in the floor curve which is absent from the ELF spectrum. At point (b), which coincides with window 3, there is a bump in the ELF curve which is produced by neutrons scattered from the detector moving mechanism. Apart from this bump, the ELF curve shows a steady reduction with time in the number of scattered neutrons or gamma rays compared to the floor station curve.

While the time spectra show the difference in total count rate from scattered particles, the pulse height spectra provide information about the relative count rates of neutrons and gamma rays, and also about the neutron energies. To illustrate how the analysis is done, pulse height spectra from the 570 keV neutrons (window 1) and from a gamma-ray source are shown in Figure 5. Provided the gamma-ray energy is higher than a few hundred keV, there is very little change in the shape of the spectrum with gamma-ray energy when the amplifier gain is set high, as was the case in this measurement. When comparing two pulse height spectra, the ratio of the gamma-ray count rates is simply the ratio of the counts in the spectra that are higher than the upper edge of the neutron spectrum in Figure 5. Similarly, the ratio of neutron counts may be compared by taking the ratio of the integrals over the lower pulse height half of each spectrum after subtracting the gamma-ray counts.

Table 1 summarises the data from the six time windows, giving the neutron energies which would have been observed if the neutrons had travelled directly from the target, together with the energies actually observed. Also given are the total counts in each window as a percentage of the counts in the neutron peak (window 1), and the ratios of the counts at the floor station to the counts at the ELF for gamma rays and neutrons at each time window.

Three major points emerge from the data in Table 1. Firstly, the neutron energies in windows 3 to 6 are much higher than the energies

calculated by the time of flight from the target, confirming that these neutrons are source neutrons which have been scattered on their way to the detector. It then follows (ignoring window 3 for the reasons given above) that the number of scattered neutrons detected on the ELF is about a factor of four less than the number detected at the floor station. Finally, using the ELF, the number of scattered gamma rays is reduced by about a factor of six.

Figure 4 shows that even greater improvements in background levels could readily be achieved by moving some of the more substantial items of the ELF, such as the detector moving mechanism and the safety rail, further away from the target.

4. ANCILLARY EQUIPMENT

The location and approximate sizes of equipment associated with the ELF are shown in Figure 6. The scale is set by the 100 mm diameter flight tube at the upper left. The major items involved in the time-of-flight measurements are described below.

4.1 Beam Pickoff

Inside the pickoff chamber, illustrated in Figure 6, is a 12 mm diameter water-cooled aperture, followed by an insulated cylinder 20 mm long by 15 mm diameter which serves as the pickoff, and a second 12 mm diameter aperture. The length of the chamber is a compromise to obtain both a satisfactory signal level and a fast rise time. In this case, signals of a few millivolts are obtained with rise times ranging between 0.8 ns for 3 MeV protons and 1.4 ns for 2 MeV deuterons.

The signal from the pickoff is required to serve both as a timing signal and as a beam pulse shape monitor to permit adjustment of the accelerator controls for an optimum pulse shape. The latter requirement imposes a more stringent requirement by demanding a low input capacitance to achieve a high input signal but a time constant which is long compared to the duration of the beam pulse. A Tektronix P6045 FET probe has the high input resistance (100 kΩ) and low capacitance (3 pF) needed to give faithful reproduction of pulses with widths in the range 3 to 100 ns.

4.2 Target Holder

The target holder has been designed to combine versatility and low scattering. A 150 mm diameter disc is mounted off-axis on the end of the flight tube (Figure 6). By rotating this disc, the centre of any one of three 25 mm diameter holes in the disc can be aligned with the

beam or the flight tube axis. Two of the holes have been fitted with 150 mm long by 25 mm diameter tubes to the ends of which a target can be fixed. The third hole is usually covered by a quartz disc to assist in lining up the beam. Targets are cooled by a jet of air from a thin stainless steel tube (Figure 6). This is sufficient for beams of up to 50 μA on beryllium but lithium targets, because of their lower melting points, degrade seriously with beam currents above 10 μA.

Another important aspect of the target holder performance is the amount of neutron scattering. Calculations were made for scattering of neutrons generated by 2.3 MeV protons incident on a thin lithium target. First, it was found that about 1.4 per cent of the neutron yield at 0° could be expected to come from neutrons emitted at angles between 90 and 120° and scattered by the brass ring which supports the target disc; second, the energies of these neutrons should be in the range 180 to 280 keV. The experiment described in Section 3.2 confirmed these predictions. Window 2 of the ELF time-of-flight spectrum was chosen to examine the bump which appears in Figure 4 about 50 ns after the main neutron peak. The energy range of the window is in accord with the theory (160 to 240 keV), while the count in the window is about 1 per cent of the count in window 1 (Table 1).

4.3 Detector Angular Positioning Device

The major components of the detector angular positioning device are clearly portrayed in Figure 6. The detector is clamped to a support which can slide along a 50 mm square section aluminium tube and is insulated electrically from the tube. Flight paths between 0.5 and 2.4 m can be obtained. The square tube is welded to an 80 mm diameter tube which slopes down to a hub connected to a 40 mm diameter steel axle. A 360 tooth gear on the axle is turned by a worm gear connected by a rubber shock absorber to the shaft of a stepping motor. Backlash in the system is less than 0.25°.

The device has worked reliably and, when operated by control pulses from a computer, can repeatedly traverse angles between + 150° and -150° with an accuracy of better than one half degree. The position can be determined by counting the number of control pulses. The only disadvantage so far encountered has been scattering of neutrons from the necessarily massive steel components of the gear housing (Section 3.2).

4.4 Neutron Flux Monitor

When measuring angular distributions or relative yields, it is

necessary to monitor the neutron flux from the target for each measurement. Absolute yields require additionally that the total accumulated beam charge be known. In experiments conducted on the ELF to date, it has been most convenient to use a BF_3 detector as a flux monitor for each measurement, and to conduct a separate measurement to establish the relationship between the monitor count and total deposited charge for each different beam particle energy. In this way, the experiment could be programmed to run for a preset monitor count, thus giving the same statistical accuracy for each measurement, regardless of the absolute target yield.

The accuracy of the normalisation was limited by the reproducibility of the detector to monitor count ratio, which proved to have a standard deviation of 3 per cent, somewhat higher than the statistical errors in counting. No correlation could be found between the magnitude of the standard deviation and the time interval between measurements, or the count rate of the detector up to rates of 10 MHz. This eliminated any systematic errors due to long term drift or dead time effects. It was therefore assumed that a random error of 3 per cent was inherent in all normalised counts.

5. NE213 SCINTILLATION DETECTOR SYSTEM

An organic scintillator combines high neutron detection efficiency with nanosecond timing resolution. In addition, the pulse height is strongly dependent on neutron energy, which allows the scintillator to be used as an energy spectrometer. The choice of a liquid scintillator such as NE213 gives additional versatility because it offers neutron-gamma discrimination and free choice of detector shape and size. In this section, details are given of the production of a scintillation chamber and its calibration. While the discussion is based on the detector used for the measurement of the $^{9}Be(d,n)^{10}B$ reaction [Whittlestone 1976], the equipment and techniques have been applied successfully to many different scintillators.

5.1 Production and Filling of a Scintillation Chamber

A borosilicate glass chamber, with one end ground flat and polished, was found to give high and most reproducible light output. A smooth jacket of heavily aluminised Mylar sheet, wrapped loosely around the chamber as a reflector, performed as well as a magnesium oxide coating and was considerably easier to manage. Two short tubes located on the side of the chamber (Figure 7) were used for filling, and provided a

small space filled with nitrogen gas to allow for thermal expansion. These tubes were terminated with standard B5 ground glass sockets which were stoppered and sealed with low vapour pressure epoxy based resin after the chamber was filled.

The filling operation was complicated by the need to keep oxygen out of contact with the scintillator liquid. Figure 7 shows a schematic diagram of a rig which permits filling of a chamber after de-oxygenation of the scintillator reservoir and flushing of the tubes and scintillation chamber with nitrogen gas. The filled chamber was removed from the rig and stoppered in a draught of nitrogen gas.

The rig proved easy to operate and the filled chambers performed very well. In particular, uniformly good pulse shape discrimination was obtained, proving that the scintillator was free from impurities such as oxygen which have a high affinity for electrons. These impurities provide a de-excitation mechanism for the long-lived triplet states responsible for pulse shape discrimination [Klein 1973]. The energy, which should be transmitted as a photon, is transferred to the impurity and pulse shape discrimination is lost.

5.2 Threshold Determination

The efficiency of an organic scintillation detector is strongly dependent on the lower level threshold. Since fast constant fraction triggers seldom have a well defined threshold, it is necessary to gate the data accumulation system with a lower level threshold defined by a properly shaped and amplified linear signal. Figure 8 shows the arrangement used by the author, based on the ORTEC 271 constant fraction timing photomultiplier base, and modified to accept a test pulse input to the linear signal preamplifier. This provides not only a check on the gain and linearity of all the linear signal processing units, but also a quick and accurate means of setting the threshold.

To set the threshold, the first step is to calibrate the pulser output against the photopeak of the 59.54 keV gamma ray from ^{241}Am. Any desired threshold may then be selected by adjusting the pulser to produce a pulse height corresponding to the required threshold energy and by setting the discriminator so that the count rate is just half the pulse rate.

5.3 Efficiency Measurement

The efficiency of the NE213 50 mm diameter x 36 mm detector was measured for a neutron energy range 50 keV to 10 MeV at a threshold

setting corresponding to an electron energy of 13 keV. Three steps were involved.

Firstly, an associated particle rig [Jones *et al*. 1974] established the absolute efficiency of the detector between 1.9 and 3.2 MeV. Next, the efficiency was calculated on the basis of proton response data by Smith *et al*. [1968] using a Monte Carlo code developed by Clayton [1976]. It was found that at energies greater than 1 MeV the calculated efficiency curve had the same shape as the measured curve, but was 4 per cent higher. Accordingly, the calculated values were adjusted downwards by 4 per cent over the range 1 to 10 MeV. To cover the energy range below 1 MeV, where calculations have yet to achieve good agreement with experiment, a relative efficiency measurement was made comparing the responses of the scintillation detector and a long counter [de Pangher 1966] exposed to monoenergetic neutrons. The relative efficiency curve was normalised to the absolute efficiency curve at 1.2 MeV.

Figure 9 shows the absolute efficiency over the range 0 to 10 MeV. Although the accuracy of the curve between 1.9 and 3.2 MeV (the associated particle measurement range) is 3 per cent, an overall accuracy of 5 per cent is claimed down to 200 keV.

6. DATA COLLECTION SYSTEM

A block diagram of the data collection system is given in Figure 8.

The PDP7 computer was programmed to control all the basic experimental operations automatically. Initially, a set of instructions such as 'stop data taking', 'type scalers', 'move detector', *etc*. was entered. The instructions would then be executed either on receipt of a pulse at an input register interfaced to the computer or on overflow of a selected scaler.

The command to move the detector caused the computer to select the next position on a list entered at the start of the experiment. Two bits on an output register activated a stepping motor control unit which provided pulses for motor control and also for an input register on the computer to enable it to keep track of the detector position.

Other useful features of the computer program were data transfer instructions and a versatile live display, with light pen control of the X axis scale and marker positions. These facilities gave the experimenter real time monitoring of the experiment and comparison of data by overlaying data regions on the display.

7. ACKNOWLEDGEMENTS

The author gratefully acknowledges the contribution of many professional and technical staff to the project. Particular mention should be made of Dr A.I.M. Ritchie for valuable discussions, Mr H.J. Fraser for design, and Mr W. Hill for construction of the post-acceleration deflection unit. The elevated target facility was designed and built by Messrs A. van Heugten and H. Broe. Useful contributions to the computer hardware were made by Messrs P.J. Ellis and M.D. Scott, while Mr R.J. Cawley was responsible for the programming.

8. REFERENCES

Clayton, E. [1976] - Neutron detector efficiency calculations for organic scintillators. 2nd National Congress, Aust. Inst. Phys., Sydney, August.

de Pangher, J. [1966] - BNWL-260.

Fraser, H.J., Ritchie, A.I.M. & Whittlestone, S. [1968] - *Rev. Sci. Instrum.*, 39 : 240.

Jones, D.T.L. & Bartle, C.M. [1974] - *Nucl. Instrum. Methods*, 118 : 525.

Klein, J. [1973] - *Nucl. Instrum. Methods*, 112 : 117.

Moak, C.D., Good, W.M., King, R.F., Johnson, J.W., Banta, H.E., Judish, J. & du Preeze, W.H. [1967] - *Rev. Sci. Instrum.*, 35 : 672.

Ritchie, A.I.M. & Fraser, H.J. [1973] - *Nucl. Instrum. Methods*, 109 : 137.

Smith, D.L. Polk, R.G. & Miller, T.G. [1968] - *Nucl. Instrum. Methods*, 64 : 157.

Whittlestone, S. [1976] - AAEC/E399.

Whittlestone, S. [1977] - *J. Phys. D.*, (in press).

TABLE 1

COMPARISON OF ELEVATED AND FLOOR MOUNTED TARGET STATIONS

Time Window	Neutron Energy (keV)		Ratio of neutron counts to neutron counts in window 1		Ratio of neutron counts Floor/ELF	Ratio of gamma counts Floor/ELF
	From time-of-flight after gamma flash	From pulse height spectrum*	ELF	Floor		
1	540	540	100	100	1.0	-
2	200	240±30	0.899	0.969	1.07	5.7
3	76	380±50	0.207	0.219	1.06	5.9
4	50	335±40	0.152	0.457	3.0	5.8
5	37	270±35	0.088	0.340	3.8	6.5
6	32	270±35	0.076	0.312	4.1	7.0

* *These energies have been calculated using the scintillator response data by Smith et al. [1968], the calibration of the pulse height scale being taken from the response to the 540 keV neutrons. The energy is the maximum observed, there being a high proportion of lower energy neutrons present.*

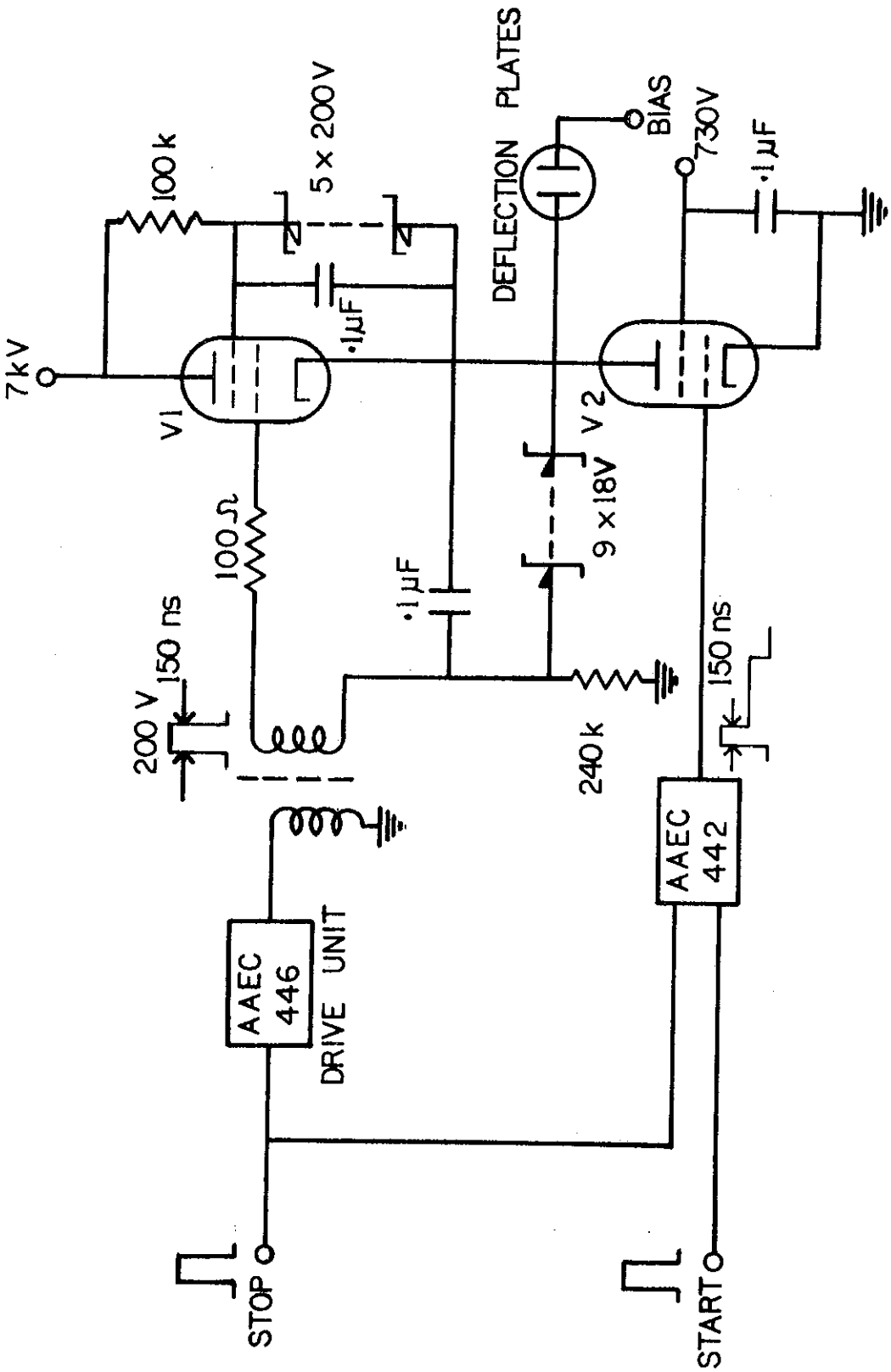

FIGURE 1. THE POST ACCELERATION DEFLECTION SYSTEM

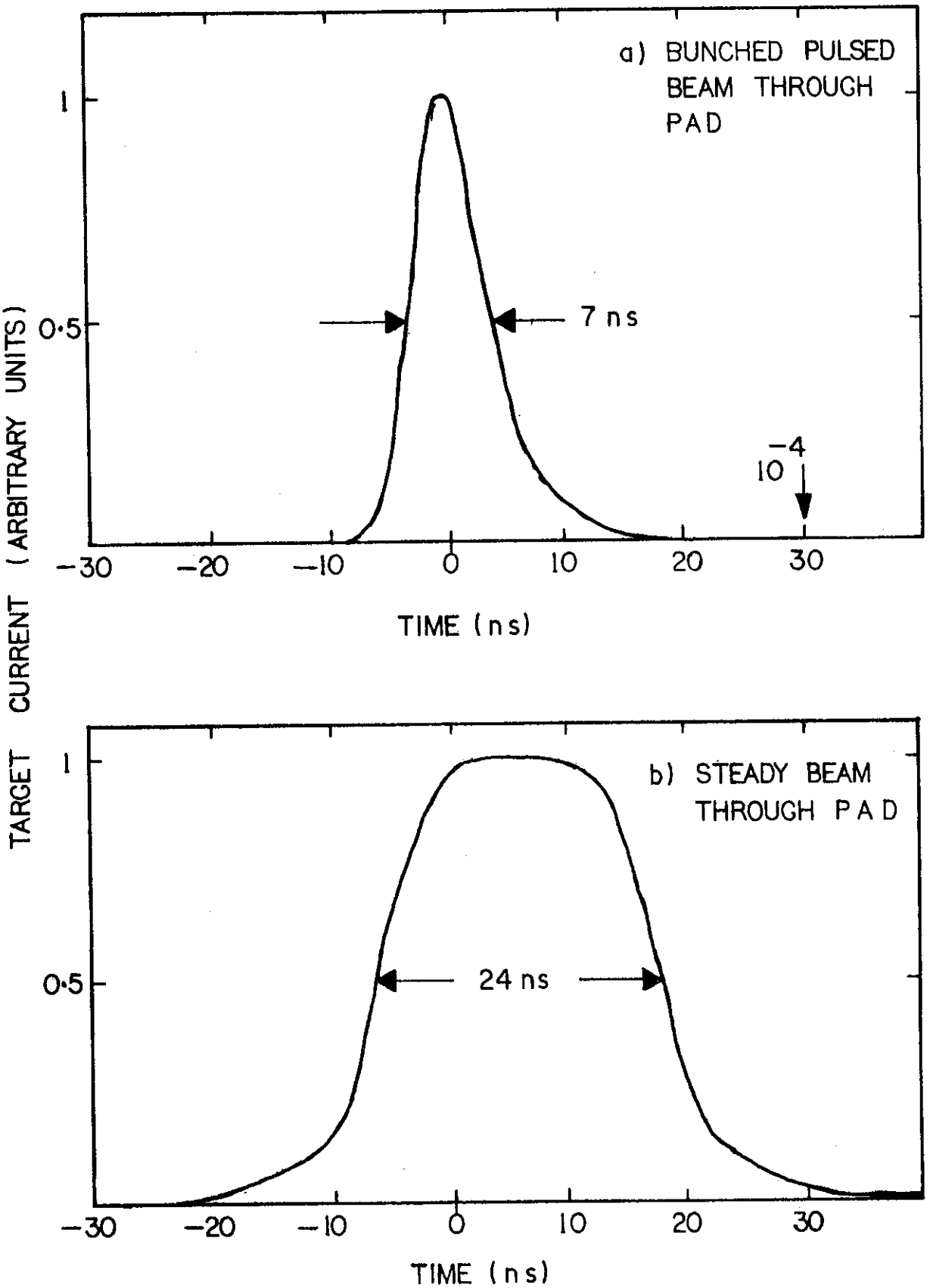

FIGURE 2. BEAM PULSE TIME PROFILES WHEN USING THE PAD

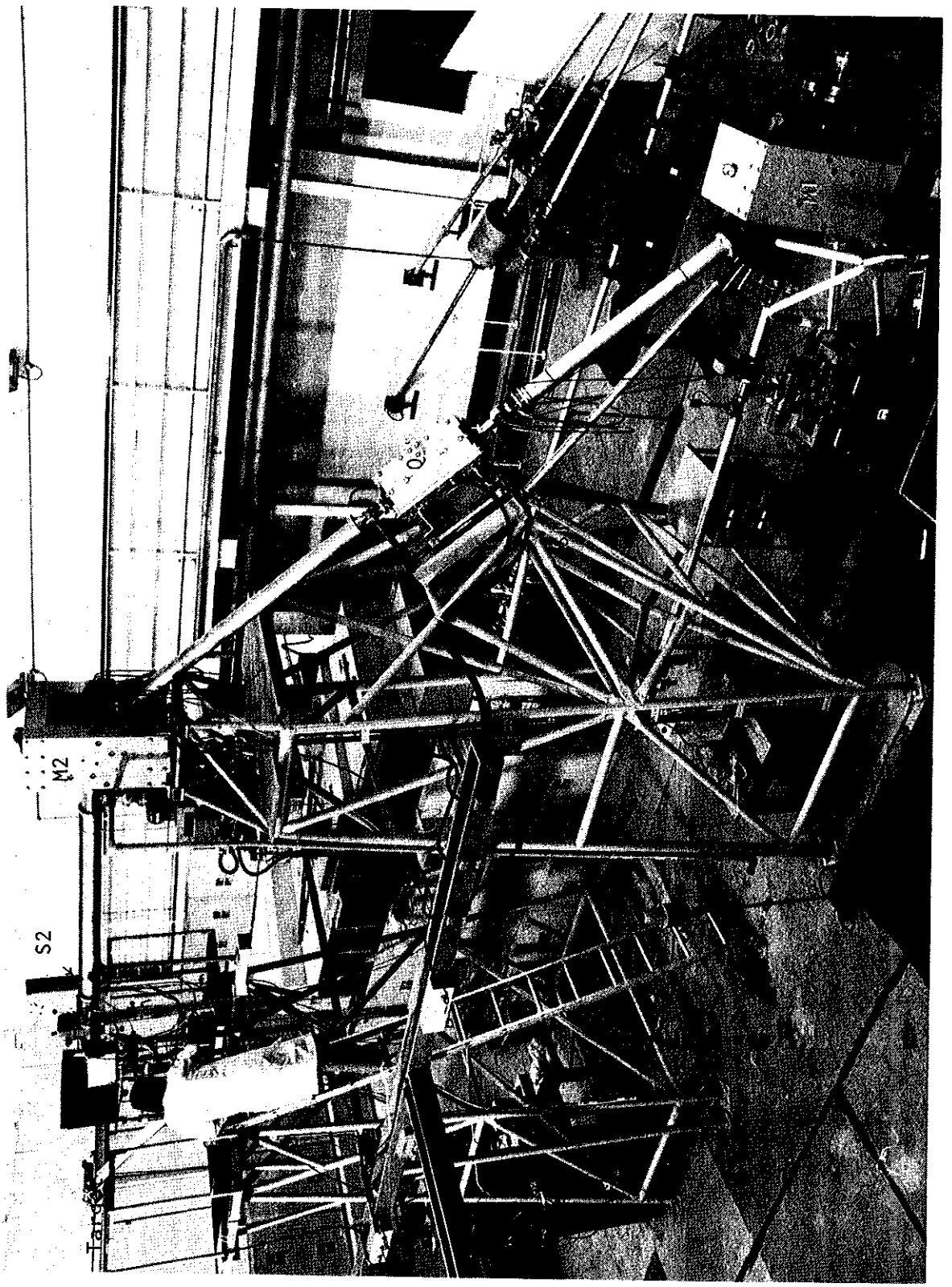

FIGURE 3. THE ELEVATED TARGET FACILITY

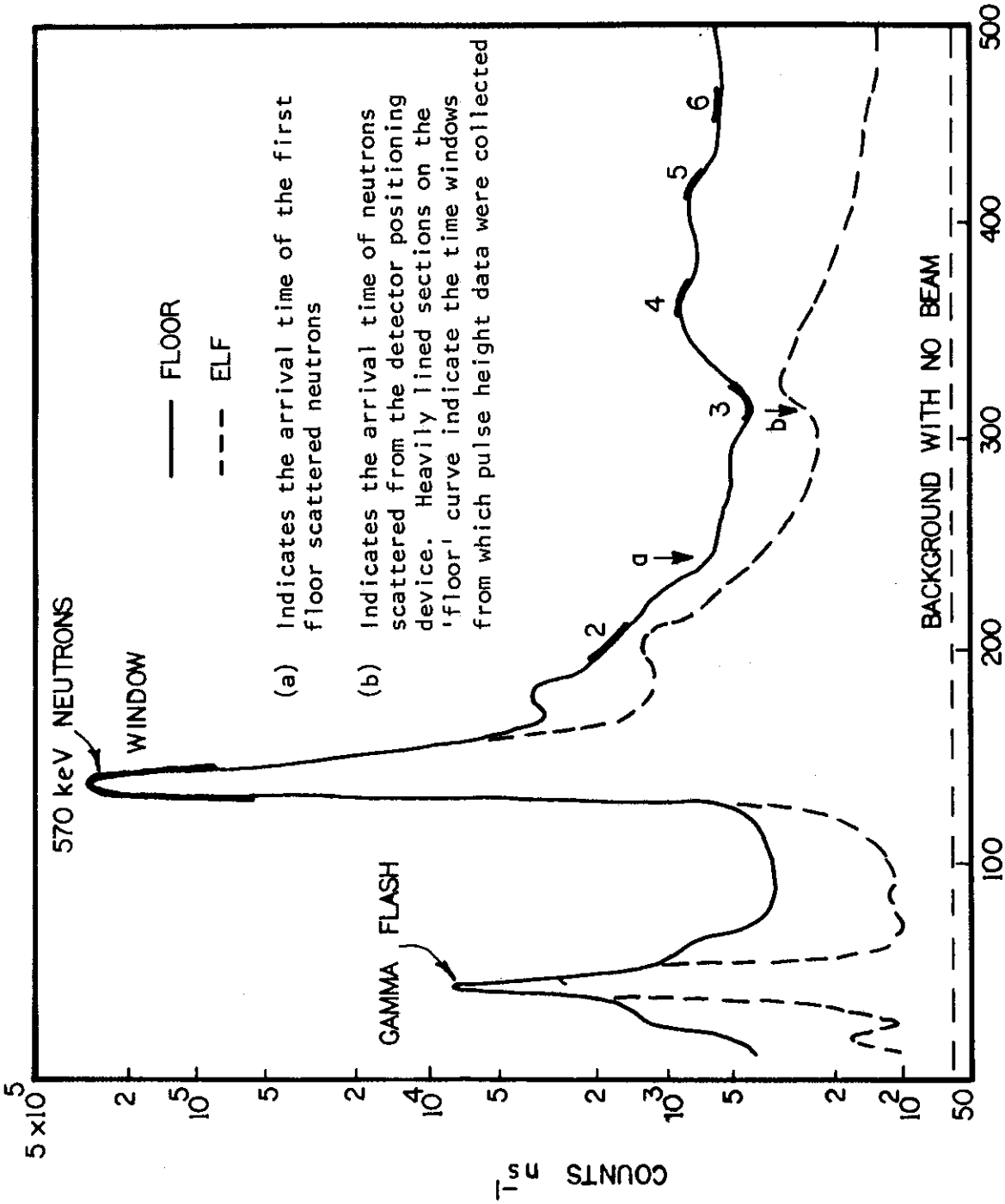

FIGURE 4. TIME SPECTRA OBTAINED FROM NE213 DETECTOR 1.033 m FROM THE ELF AND GROUND FLOOR TARGETS

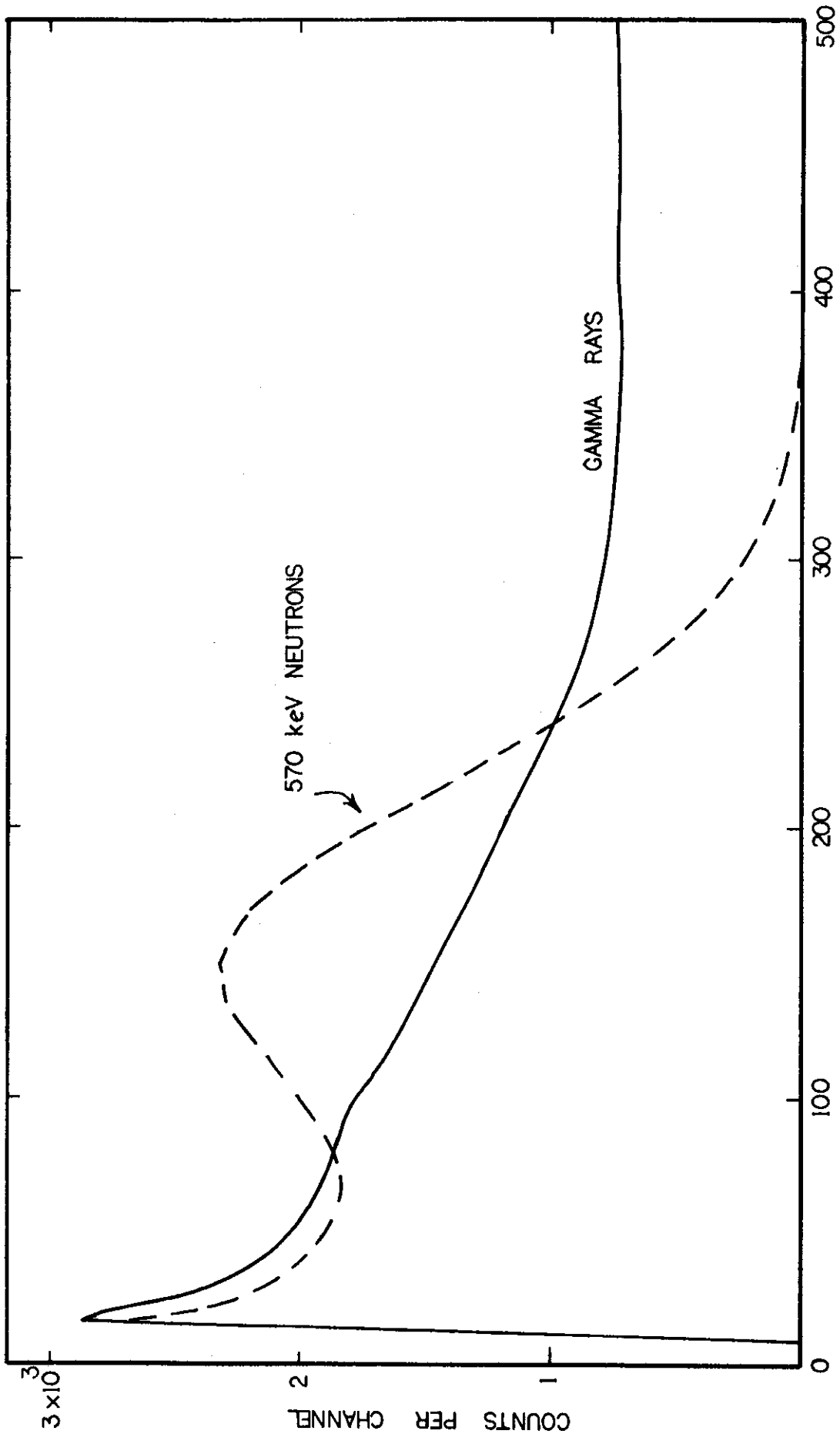

FIGURE 5. PULSE HEIGHT SPECTRA FROM NEUTRONS AND GAMMA RAYS

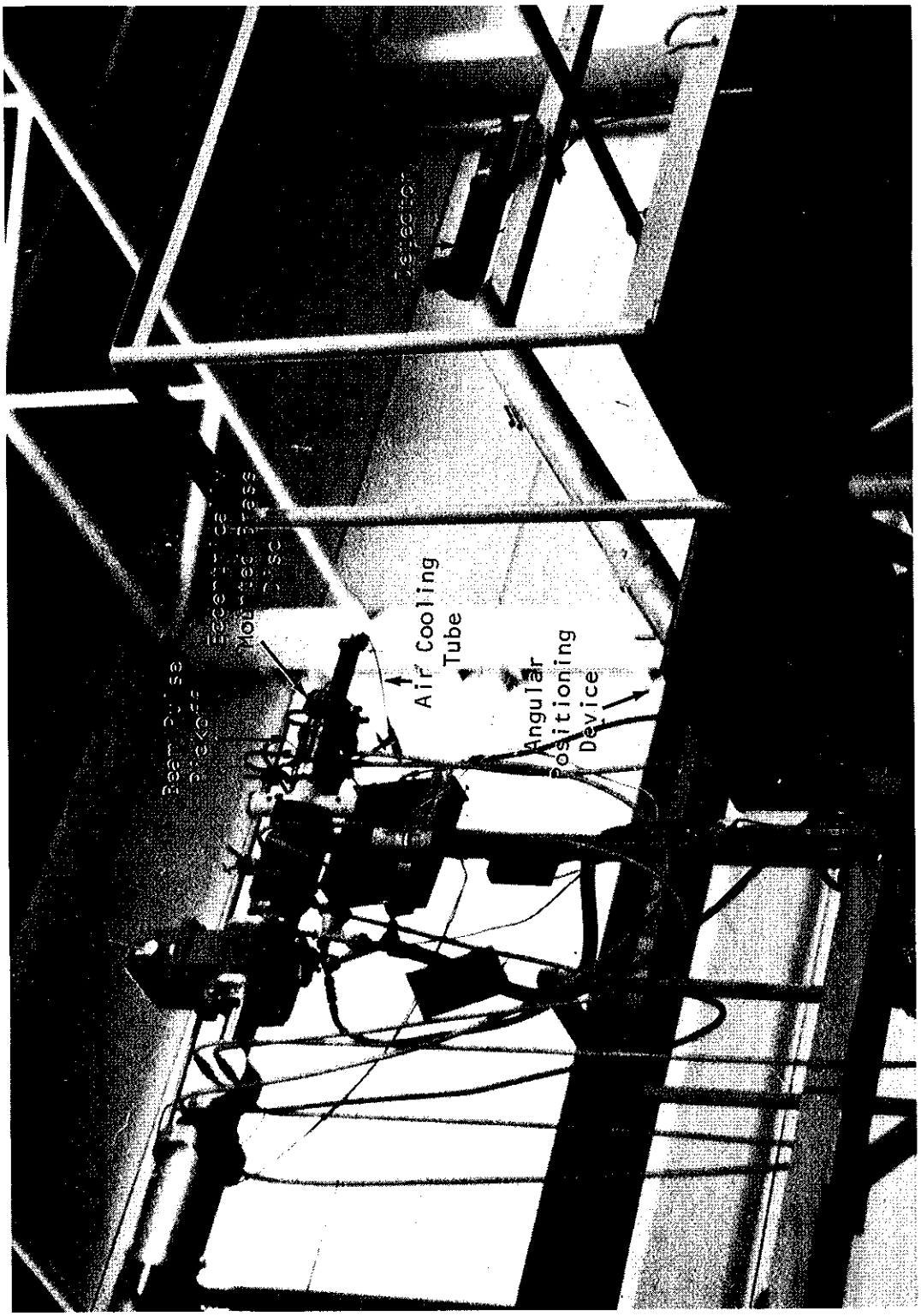

FIGURE 6. THE ELEVATED TARGET FACILITY STATION

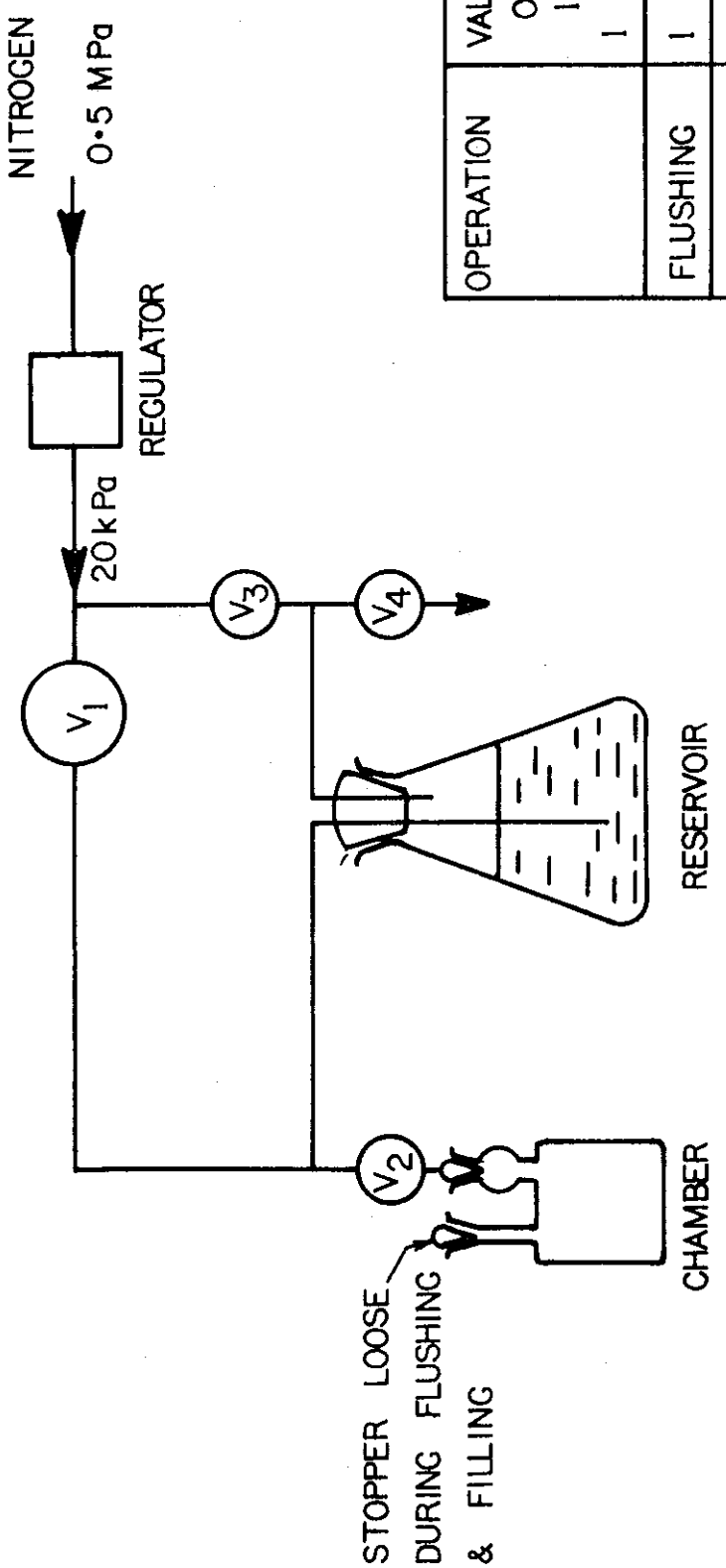

OPERATION	VALVE SETTING 0 = CLOSED 1 = OPEN 1 2 3 4		
FLUSHING	1 ·5	0	·5
FILLING	0 FOR CONTROL	USED	1 0

FIGURE 7. LIQUID SCINTILLATION DETECTOR FILLING RIG

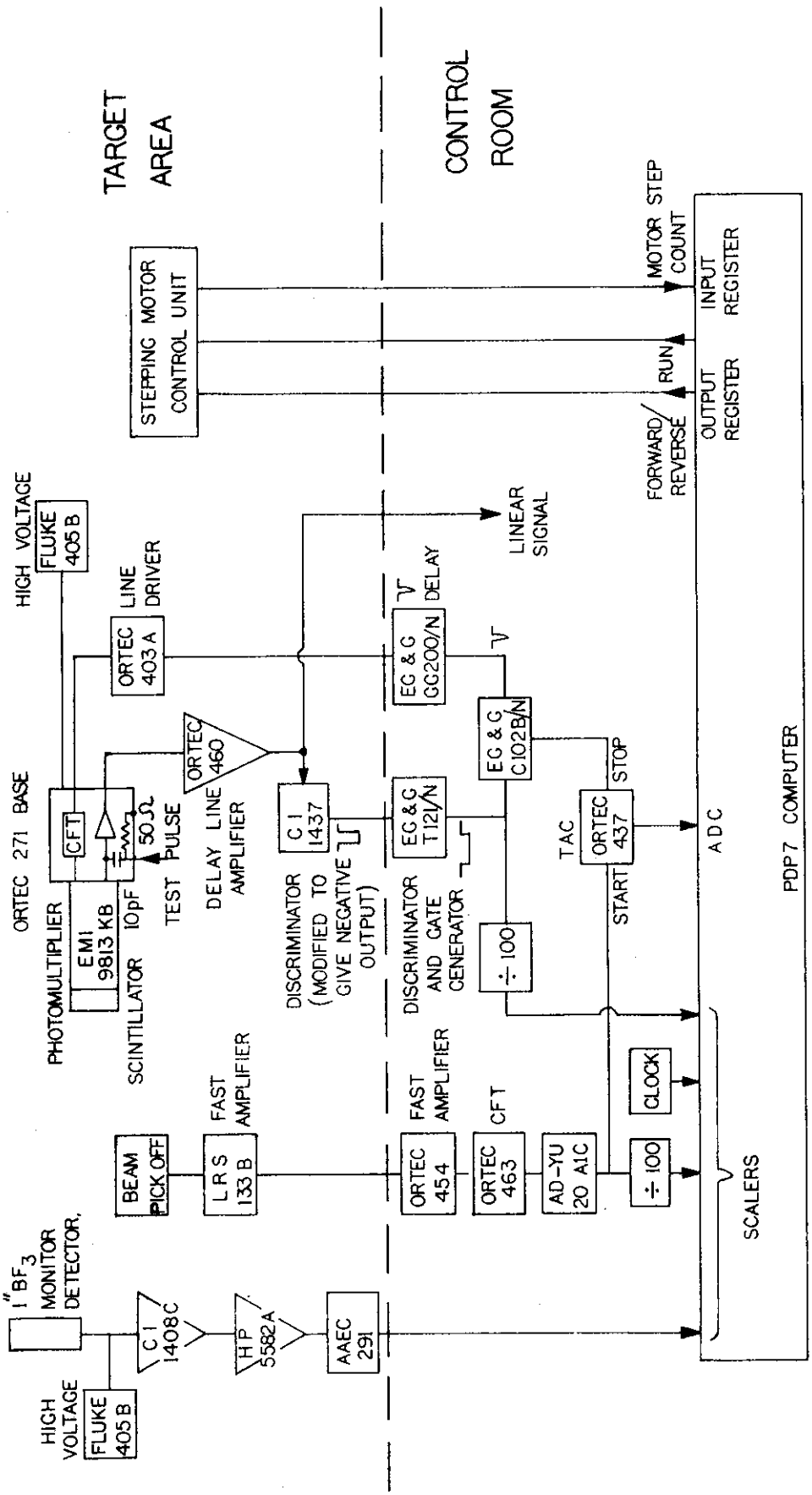

FIGURE 8. ELECTRONICS FOR THE NEUTRON TIME-OF-FLIGHT MEASUREMENT

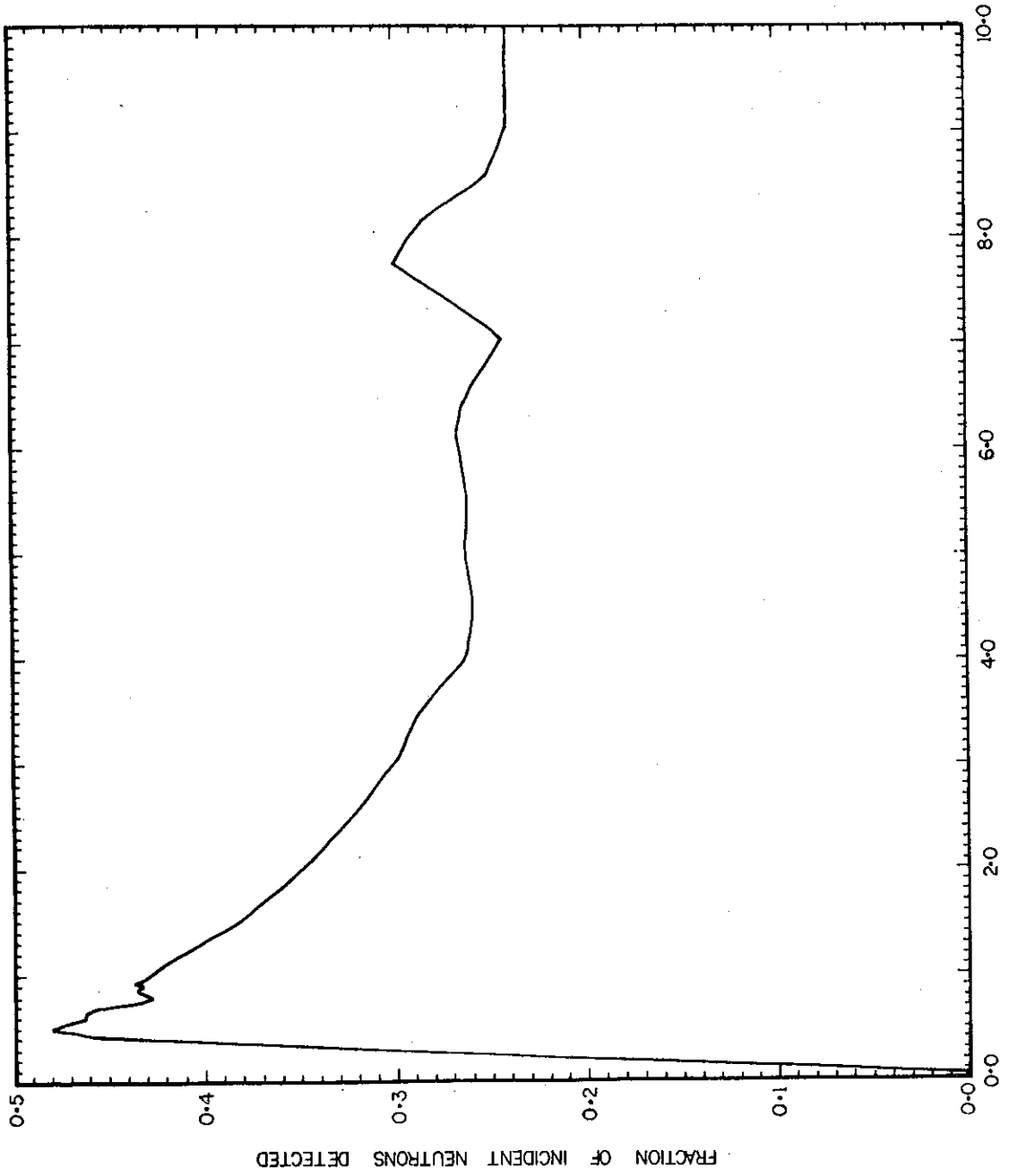

FIGURE 9. ABSOLUTE EFFICIENCY OF THE NE213 LIQUID SCINTILLATION DETECTOR